Progress In Electromagnetics Research B, Vol. 63, 145–160, 2015

Moving Target Detection by Using New LTE-Based Passive Radar

Raja S. A. Raja Abdullah[1, *], Asem A. Salah[1], and Nur E. Abdul Rashid[2]

Abstract—This paper examines the feasibility of Long Term Evolution (LTE)-based passive radar for detecting ground moving targets. Specifically, the focus of this paper is to describe the proposed LTE-based passive radar system and to conduct an experiment using a real LTE eNB transmitter as an illumination source. Seven scenarios were carried out to investigate the detection performance of the proposed system on ground moving targets with different speeds, trajectories and range. In addition, multi-target detection was also tested. The experimental results showed that the LTE-based passive radar system has the capability to detect typical ground targets like cars, motorbikes and humans moving at different trajectories. LTE is a new communication system and very few experimental result with real LTE signal has been published, thus the result and analysis from this paper will complement the technical readiness of the so called LTE based passive Radar. The positive results opened up a new frontier for passive radar systems to be used in many potential applications, including security, border protection, microwave fences, monitor of buildings and others.

1. INTRODUCTION

A passive radar system is made up of a receiver without a co-located transmitter. It has advantages over the conventional radar system in many ways. For example, it is practically invisible to surveillance, it is easily transported due to its small size and it is cheaper as it does not transmit any signals. Recently, the use of illuminators of opportunity by passive radar systems has gained the interest of radar engineers and researchers. As a result, illuminators have been employed from various sources, such as television broadcasting [1], FM radio [2], digital video (DVB) and audio (DAB) broadcasting [3], satellites [4], wireless fidelity (WiFi) [5, 6], global systems for mobile communications (GSM) [7, 8] and worldwide interoperability for microwave access (WiMAX) [9, 10].

However, the Long Term Evolution (LTE) is one of the latest wireless communication technologies, which provides last-mile broadband wireless access with anticipated widespread accessibility. An LTE signal presents interesting properties which provide a huge motivation to use it as an illuminator of opportunity for passive radar systems such as:

- Broad bandwidth within the range of 1.4–20 MHz which allows it to have high range resolutions.
- Large frequency bands ranging from 800–3500 MHz as well as its ability to support both frequency division duplex (FDD) and time division duplex (TDD) [11], which enhances the opportunity of LTE to be deployed in many countries.
- LTE uses Orthogonal Frequency Division Multiple access (OFDMA) which guarantees low side-lobes of the ambiguity function.

The above mentioned LTE signal characteristics and other factors had motivated this research group to study the feasibility of LTE signals as the new illuminator of opportunity for passive radar applications for the first time as in [12], where the LTE signal was fully analysed based on the range,

Received 9 July 2015, Accepted 31 August 2015, Scheduled 1 September 2015

* Corresponding author: Raja Syamsul Azmir Raja Abdullah (r_syamsul@upm.edu.my).

[1] Wireless and Photonic Networks Research Centre, Faculty of Engineering, Universiti Putra Malaysia (UPM), Selangor 43400, Malaysia. [2] Faculty of Electronic & Electrical Engineering, Universiti Teknologi MARA (UITM), Shah Alam Selangor, Malaysia.

Doppler ambiguities and resolutions. The results showed that the LTE signal is attractive to be used for passive radar applications since it can achieve a good range and Doppler resolution of 8.6 m and 0.132 m/s, respectively. These preliminary results motivated us to continue to conduct an experimental investigation into the feasibility of LTE waveform for passive radar [13], where analytical analysis was conducted on a captured LTE signal in the atmosphere (received from real LTE eNB). Despite the positive results shown, there is still the need for experimental studies to investigate LTE-based passive radars' capability of detecting moving targets. Therefore, this paper intends to deploy and investigate the performance of LTE-based passive radar for detecting:

- Moving targets with different speeds.
- Moving targets with changeable trajectories.
- Multi-targets in the same scene.

The results complemented the gaps within the passive radar system study and can be useful for more advanced practical passive radar systems with high resolution requirements. The paper is organised as follows: Section 2 analyses the characteristics of LTE waveform for radar applications in terms of range and Doppler resolution. The SNR calculation for LTE signal propagation is presented in Section 3. The proposed LTE-based passive radar system architecture is illustrated and explained in Section 4. The experimental results and discussions for the 9 conducted scenarios are presented in Section 5 and conclusions are made in Section 6.

2. RANGE AND DOPPLER RESOLUTIONS IN LTE PASSIVE RADAR

In bistatic passive radar applications, the minimum range separation required between two targets is called the range resolution, ΔR, where the two targets are assumed to be co-linear with the bistatic bisector. Range resolution is defined as [12, 14].

$$\Delta R = c/\left(2B\cos(\beta/2)\right) \tag{1}$$

where B and c are the signal bandwidth and light velocity respectively. β is the bistatic angle, which is defined as the angle between the transmitter and receiver with the vertex at the target [15]. From (1), range resolution is shown as a function of bandwidth B. The larger the bandwidth of the waveform used in the radar, the better the range resolution. Meanwhile, according to the 3GPP release 8, the bandwidth of the LTE signal may range from 1.4 to 20 MHz. Therefore, 8.6 m of the range resolution can be reached using a bandwidth of 20 MHz and $\beta = 60°$. The LTE signal has better range resolution as compared to other illuminators of opportunity, as it helps to identify two close targets efficiently.

The Doppler resolution determines how well a radar can observe targets of different radial velocities. It can be determined from the receiver's coherent integration time (CIT), where the adequate degree of Doppler separation between two targets echoes at the receiver is given by [12, 15]:

$$\Delta f_d = f_{dT1} - f_{dT2} = 1/T \tag{2}$$

Δf_d is the Doppler resolution and T the CIT. f_{dT1} and f_{dT2} are the received Doppler echoes from the first and second targets, respectively, and they are defined as [18]:

$$f_{dT1} = 2v_{T1}\cos(\alpha_1)\cos(\beta/2)/\lambda \tag{3}$$

$$f_{dT2} = 2v_{T2}\cos(\alpha_2)\cos(\beta/2)/\lambda \tag{4}$$

The geometry for target 1 and target 2 velocities v_{T1} and v_{T2}, respectively, is shown in Figure 1 where α_1 and α_2 are the velocity radial angle for target 1 and target 2 respectively. The two targets are assumed to be co-located so that they share the same bistatic bisector. Combining Equations (2), (3) and (4) yields:

$$\Delta f_d = 2\cos(\beta/2)\left(v_{T1}\cos(\alpha_1) - v_{T2}\cos(\alpha_2)\right)/\lambda \tag{5}$$

The required difference between the two target velocity vectors projected onto the bistatic bisector is known as velocity resolution Δv and it is given as [18]:

$$\Delta v = v_{T1}\cos(\alpha_1) - v_{T2}\cos(\alpha_2) \tag{6}$$

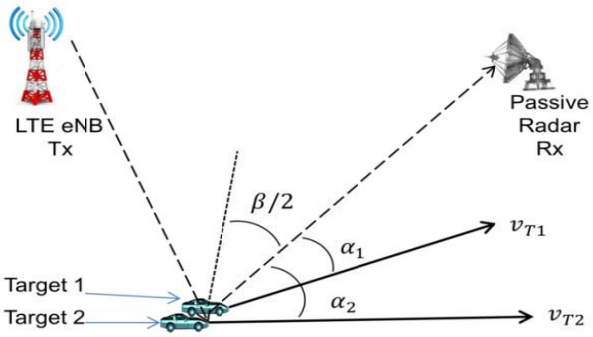

Figure 1. Geometry for bistatic Doppler resolution.

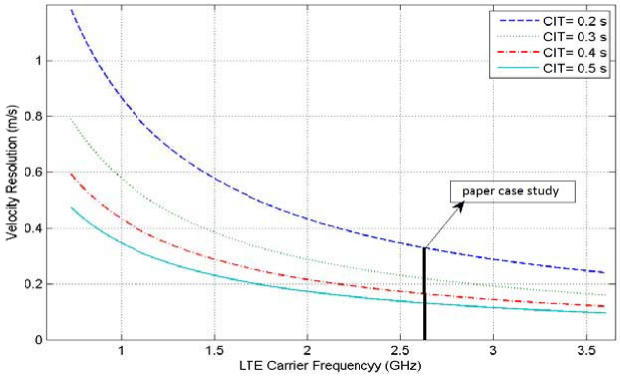

Figure 2. Velocity resolution with difference CIT for LTE signal.

Then by combining Equations (5) and (6), the velocity resolution becomes:

$$\Delta v = \lambda / \left(2T \cos(\beta/2)\right) \tag{7}$$

As an example, in this paper, the adopted CIT is 0.2 s, and the Δf_d is calculated to be 5 Hz, corresponding to the velocity resolution of 0.288 m/s if $\beta = 60°$ and $f_c = 2.635$ GHz are used. Therefore, the LTE-based passive radar system can distinguish two targets moving with a velocity difference of 0.288 m/s. Figure 2 shows the velocity resolutions of different CIT values and different frequency carriers defined by LTE. From Figure 2, it is clearly shown that the velocity resolution improves as the carrier frequency increases. Considering this case study where the LTE carrier frequency is 2.635 GHz, by increasing the CIT to 0.5 s, the LTE signal can achieve a velocity resolution of 0.1322 m/s which is considered as a good Doppler resolution that makes the LTE-based passive radar suitable for moving target indication applications.

3. SNR AND POWER LINK ANALYSIS FOR LTE BASED PASSIVE RADAR

To estimate the received signal power in a free space propagation model, ideal propagation condition with clear line-of-sight (LOS) is assumed in this paper. The received signal power can be calculated from a Friis equation [15, 16]:

$$P_r = P_t G_t G_r \lambda^2 / (4\pi)^2 d^2 \tag{8}$$

where P_t is the transmitted power. G_t and G_r are the antenna gains for the transmitter and receiver, respectively, and λ is the wavelength. However, when the receiver is close to the ground, the two-ray ground reflection model is considered where the total received power can be modeled as the vector sum of the direct transmitted signal and one ground reflected signal. The same assumption is considered for when the total signal power hits the ground targets, which is considered in this paper. The two signals are added constructively or destructively depending on their different phases at the receiver, where the phase and magnitude of direct transmitted signal varies with distance travelled, while the magnitude of reflected signals depends on the total travelled signal in addition to the reflection coefficient (Γ related to the signal before and after reflection [16].

Figure 3 shows the LTE transmission with a ground reflection diagram and from the figure, the received line of sight (LOS) signal power can be written as [15, 16]:

$$P_{\text{los}} = P_t G_t G_r \lambda^2 / (4\pi R_{\text{los}})^2 \tag{9}$$

R_{LOS} is the LOS distance between the transmitter and the receiver antennas and given by:

$$R_{\text{los}} = \sqrt{\left((h_t - h_r)^2 - d^2\right)} \tag{10}$$

The ground reflected signal power may be written as [15, 16]:

$$P_{refl} = P_t G_t G_r \lambda^2 / (4\pi R_{refl})^2 \Gamma \tag{11}$$

R_{refl} is the total distance for the ground reflected signal, and it is given as:

$$R_{refl} = \sqrt{\left((h_t + h_r)^2 - d^2\right)} \tag{12}$$

When a radio signal hits a junction between different dielectric media, a portion of energy passes through the junction while the remaining energy is reflected. The incident angle, signal polarization, different permeability (μr), dielectric (εr), and conductivity (σ) are parameters that can affect the reflected portion energy. The reflection coefficient for the vertical polarized signal is given as [16]:

$$\begin{aligned}\Gamma_v \;=\; &\left((\varepsilon r - j60\sigma\lambda)\sin(\theta_i) - \sqrt{\left(\varepsilon - j60\sigma\lambda - \cos^2(\theta_i)\right)}\right) / \left((\varepsilon r - j60\sigma\lambda)\sin(\theta_i)\right. \\ &\left. + \sqrt{\left(\varepsilon r - j60\sigma\lambda - \cos^2(\theta_i)\right)}\right)\end{aligned} \tag{13}$$

and the reflection coefficient for the horizontal polarized signal is given as [9]:

$$\Gamma_h = \left(\sin(\theta_i) - \sqrt{\left(\varepsilon r - j60\sigma\lambda - \cos^2(\theta_i)\right)}\right) / \left(\sin(\theta_i) + \sqrt{\left(\varepsilon r - j60\sigma\lambda - \cos^2(\theta_i)\right)}\right) \tag{14}$$

Then, the total received power including the ground reflected signal is given as:

$$P_{\text{Tot\_Rec}} = P_{\text{los}} \pm \left(P_{refl} \cdot \cos(\Delta\Phi)\right) \tag{15}$$

The experiment has been conducted by using real LTE signal and system with a carrier frequency $f_c = 2.635\,\text{GHz}$, transmitted from an LTE eNB antenna located on a tower with a height of $h_t = 30\,\text{m}$ and received on an antenna with a height $h_r = 1\,\text{m}$. The LTE signal is transmitted with a transmission power of $P_t = 46\,\text{dBm}$. The estimated total power for the received signal is shown in Figure 4 where the ground reflection 2-ray model is considered. The antenna gains for the transmitter and receiver are assumed to be the same at $G_t = G_r = 1$ and $\varepsilon r = 18$. The graph in Figure 4 illustrates the effects of the ground and polarization in open field measurements. The figure shows that there is a large difference between the expected performance when the ground influence is included and the Friis transmission equation for free space. Vertical polarization is less susceptible to multipath fading than horizontal polarized signal. For long distances, the signal level predicted by the Friis equation is considerably higher than the reading that includes the ground reflection.

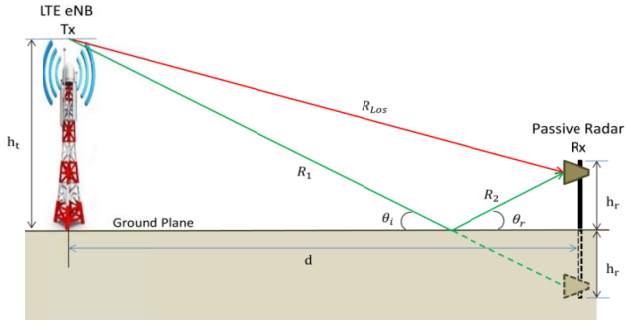

Figure 3. LTE transmission with ground reflection diagram.

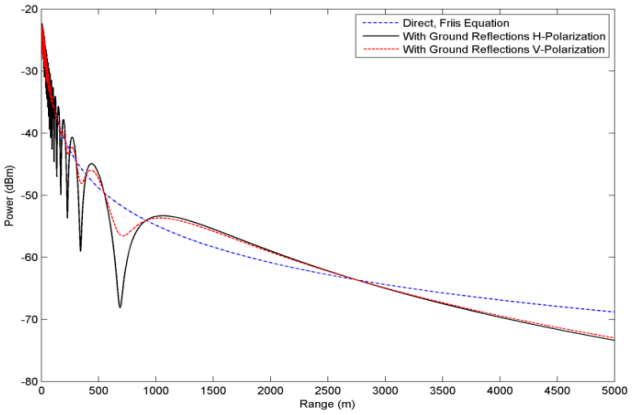

Figure 4. Friis equation compared to ground reflection model for vertical and horizontal polarization LTE signal.

To estimate the SNR for the LTE based passive radar system, the reflected signal from the object with specific radar cross section at a specified range using the point target is considered. The equation for the power at the input to the receiver is [15, 16]:

$$P_r = P_t \frac{G_t G_r \lambda^2 \sigma}{(4\pi)^3 R_t^2 R_r^2 L} \tag{16}$$

where σ is no fluctuating target radar cross section (RCS) in square meters, L is general loss factor that accounts for both system and propagation losses, R_t is range from the transmitter to the target and R_r

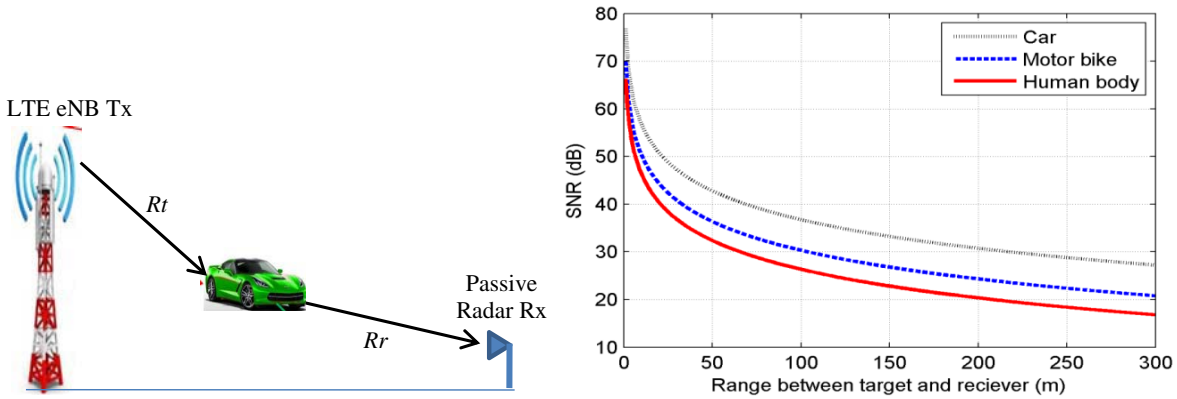

Figure 5. LTE transmission with target reflection and its SNR estimation from different targets.

is the range from the receiver to the target as shown in Figure 5. The noise is modeled by assuming the thermal noise at the receiver has white power spectral density, thus the total noise power at the output of the receiver is given by [15, 16]:

$$N = \frac{kTF_n}{\tau} \tag{17}$$

where k is the Boltzmann constant, T the effective noise temperature and F_n the receiver noise factor. Assuming that the magnitude squared receiver frequency response approximates a rectangular filter with bandwidth equal to the reciprocal of the pulse duration, $1/\tau$. The product of the effective noise temperature and the receiver noise factor which is the system temperature and is denoted by T_s so that $T_s = TF_n$. Therefore the receiver output SNR is:

$$\frac{P_r}{N} = P_t \frac{\tau G_t G_r \lambda^2 \sigma}{(4\pi)^3 k T_s R_t^2 R_r^2 L} \tag{18}$$

The estimated SNR for the signal reflected from different targets in the LTE system is shown in Figure 5. The SNR is calculated for three different targets: i) Car with RCS 2.2 m^2, ii) motorbike with RCS 0.5 m^2 and iii) human body with RCS 0.2 m^2. From Figure 5 it is clearly shown that the SNR for human body is less than the motorbike and both of them are less than the SNR of the car, corresponding to the higher RCS for the car. It is noted that the SNR is reduced as the range between the targets and receiver antenna increased.

4. LTE-BASED PASSIVE RADAR SYSTEM ARCHITECTURE

The proposed system consists of two parallel co-located channels; Ch1 and Ch2. Ch1 is dedicated to receive the direct path reference signal from the LTE eNB, while Ch2 is dedicated to receive the echo signal reflected from the targets. The receiver hardware system architecture is shown in Figure 6. The two channels have the same structure, where each channel is started by a horn antenna used to receive the LTE signal carried at the 2.635 GHz carrier. The antenna of Ch1 is directed towards the LTE eNB (LTE base station), while the antenna of Ch2 faces the area where the target should be. The antenna is followed by a low noise amplifier (LNA) which amplifies the received RF signal which the desired LTE downlink frequency band is then selected by the band pass filter (BPF). Subsequently, the desired signal is down converted to the baseband by heterodyning it with the local oscillator signal using a frequency mixer. An amplifier is used to amplify the baseband signals to provide sufficient gains for the LTE signal before filtering out the undesired frequencies using the LPF. Then, the LTE baseband signals are saved into PC hard drives with a sampling rate of 25 MS/s. A channel of the implemented experimental LTE-based passive radar system for detection is shown in Figure 6.

Both of the received signals from the direct path channel Ch1 and reflected path channel Ch2 are saved in long data sets that need huge processers which may take a long time to process. Therefore, data formatting is necessary for both channels before going through the cross-ambiguity coherent processing.

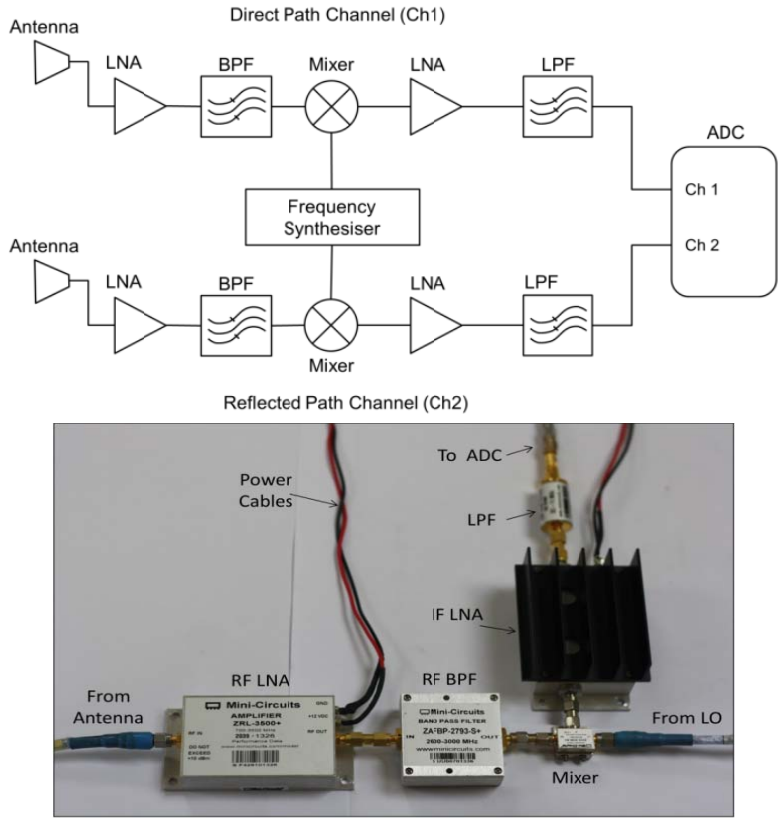

Figure 6. Architecture of experimental LTE-based passive radar system and receiver hardware for one channel.

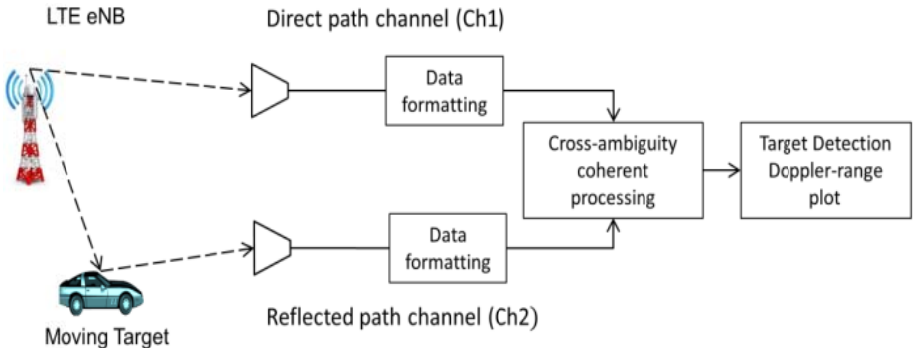

Figure 7. LTE-based passive radar signal processing scheme for target detection.

The overall signal processing scheme associated with the LTE-based passive radar is illustrated in Figure 7. The received LTE signal data are formed in segments; one segment is to be processed each time. The length of each segment will decide the CIT, and subsequently the Doppler resolution. In this paper a segment of 5 MS length is adopted, corresponding to a CIT of 0.2 s for a 25 MS/s sampling rate. Therefore, the obtained Doppler resolution is 5 Hz, corresponding to 0.3 m/s (1.1 km/h) velocity resolution with $f_c = 2.635$ GHz and $\beta = 60°$.

The two LTE signals received from Ch1 and Ch2 are uneven by two parameters, which are the time delay and Doppler shift. In fact, these two parameters will decide the range and velocity of the detected moving target. Therefore, the cross ambiguity function (CAF) is applied, which is the matched filter response to the joint time-delay and Doppler-shift version of the LTE signal it is matched to. It is given

by [17]:

$$(\tau, f_d) = \int s_r(t) \cdot s_d^*(t-\tau) e^{-2\pi f_d t} dt \tag{19}$$

where $s_r(t)$ and $s_d(t)$ are the received target echo signal and direct reference signal, respectively. Time-delay τ and Doppler-shift f_d are the two parameters to be searched for the values that cause $A(\tau, f_d)$ to peak. This can be done by delaying the direct signal $s_d(t)$ in time τ and shifting its frequency by some amount f_d, and cross-correlate it with the reflected signal $s_r(t)$, followed by searching for the maximum value of $A(\tau, f_d)$, which gives the peak. After obtaining all the $A(\tau, f_d)$ values, the Doppler-range plane is plotted in contours.

In this paper, all the detection results are illustrated in contour plots, which show the isolines of the CAF output matrix $A(\tau, f_d)$. After normalizing the CAF matrix, the contour plots are drawn with contour lines at a specified contour cut-off level V. The contour setup flowchart is shown in Figure 8. The contour cut-off level is determined based on the strongest peak detected while $f_d \neq 0$, where $V =$ the strongest peak level $-L$, and here L is chosen to be at 3 dB which allows to see one peak clearly. This

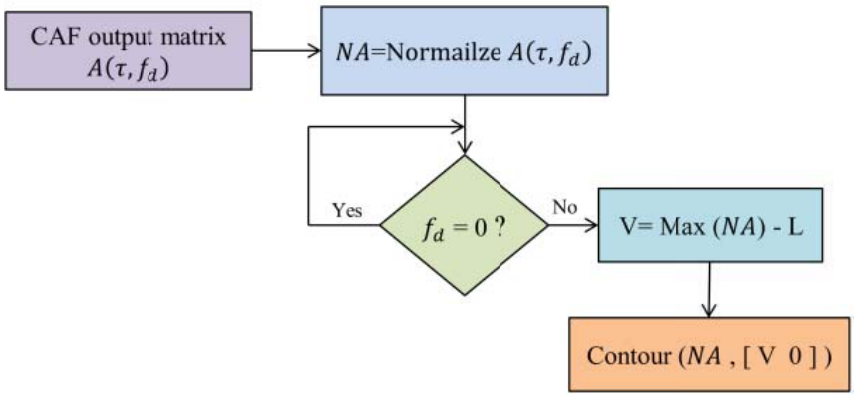

Figure 8. Contour process flowchart for the LTE-based passive radar detection.

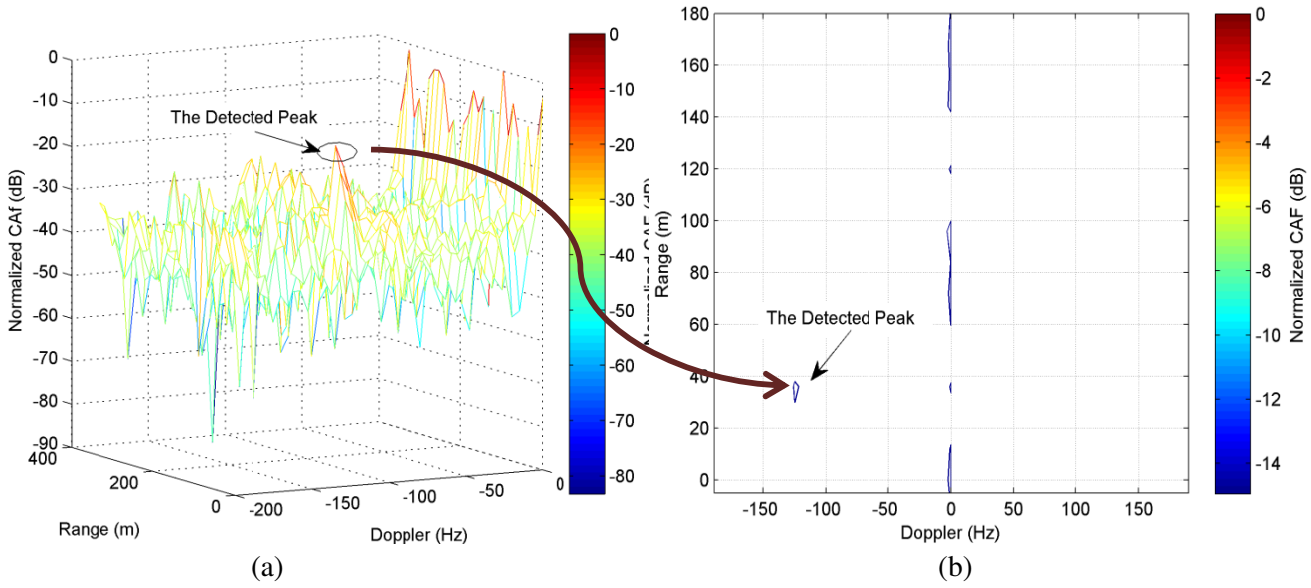

Figure 9. Example of CAF plots with one target detection scenario, (a) the mesh plot, (b) the contour plot.

means that the contour lines will be plotted for all levels from the cut-off value to the zero. Examples for the contour plot are shown in Figure 9, where Figure 9(a) shows the mesh for normalized CAF with one target detection scenario and one peak which clearly appears on the Doppler at 130 Hz, a range of 36 m, and a peak strength of ~ -12 dB. Then, the contour plot for the same CAF is drawn in Figure 9(b) which shows the contour lines from level ~ -15 dB to 0, and the peak appears at the same Doppler and range of 130 Hz and 36 m, respectively.

5. EXPERIMENTAL RESULTS AND DISCUSSION

In order to evaluate the performance and capability of the proposed LTE-based passive radar hardware system, field experiments were conducted using a selected operational LTE eNB in a huge open area. The testing site is located in a car park situated 400 m from the LTE eNB transmitter, as shown in Figure 10. The experiment site (marked as a dashed rectangle in the figure) will be used to illustrate each scenario in the following subsections. The aim of this experiment is to examine the proposed LTE-based passive radar system's capability of detecting diverse types of moving targets with different speeds and different trajectories. Nine scenarios were carried out for different types of moving targets including cars, people and motorbikes. The conducted scenarios are summarized in Table 1.

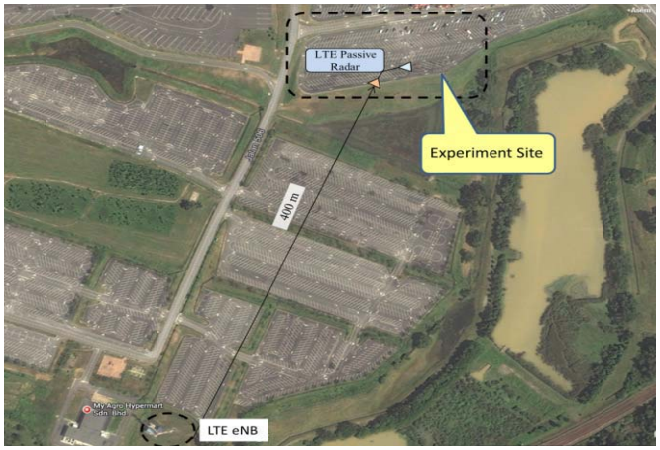

Figure 10. Experimental site geometrical aerial photo for target detection.

Table 1. Summary of the conducted scenarios.

Scenario	Scenario Description	Aim
Scenario A	One car moving in a straight line from the receiver for 140 m, with different speeds.	**Detection for different speeds**
Scenario B	One car moving from the receiver and making a back turn after 90 m.	**Detection for different trajectories**
Scenario C	Motor bike drives in a straight line from the receiver antenna for 130 m.	**Detection for different targets**
Scenario D	One person running in a straight line for 60 m away from the receiver.	
Scenario E	Two people running with different speeds moving from the receiver up to 65 m.	**Detection for multi-targets**
Scenario F	Two cars follow each other by driving in a straight line from the receiver to a 160 m distance away.	
Scenario G	Two cars and one motor bike drive away from the receiver in straight lines with different speeds.	

5.1. Scenario A

Scenario A shows a car moving in a straight line starting from the receiver's Ch2 antenna until it reached a point with a distance of 130 m at a speed of $\sim$ 30 km/h. Figure 11 shows the geometrical

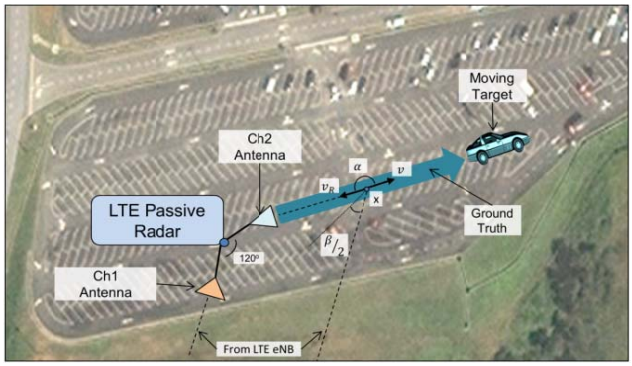

Figure 11. Geometrical configurations for the experiment site of Scenario A: car moving in a straight line from the receiver to 130 m away.

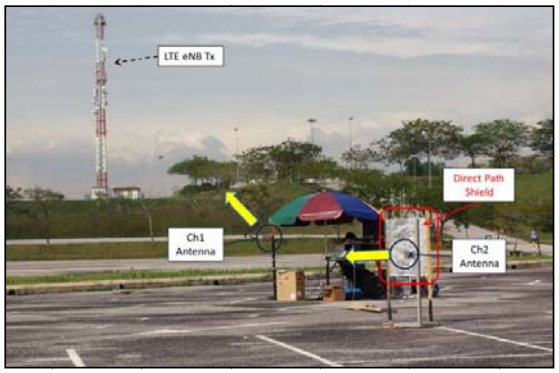

Figure 12. LTE-based passive radar field experiment setup for Scenario A.

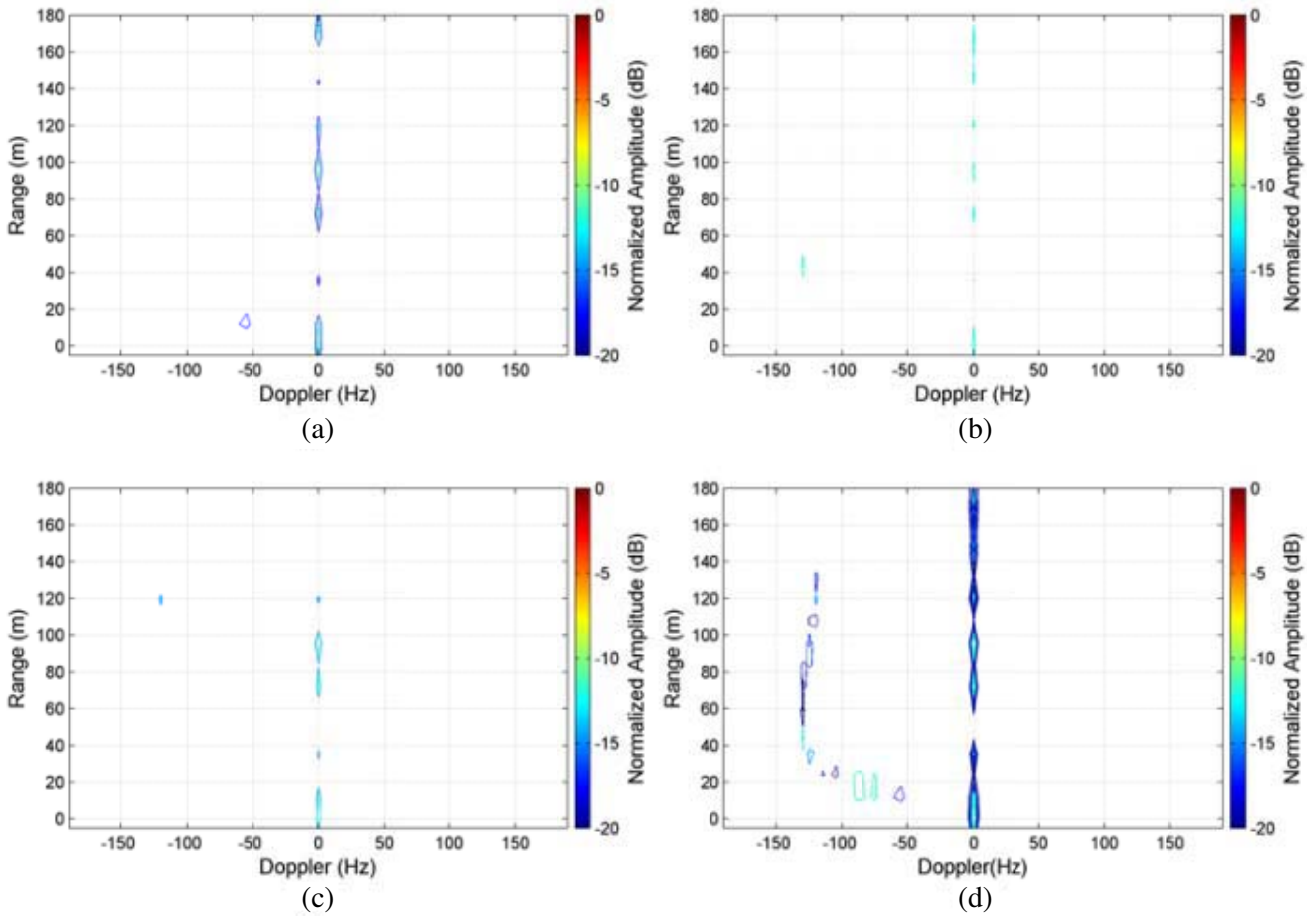

Figure 13. Scenario A, a detection processing results display in a Doppler-range contour for the (a) 1st range cell, (b) 6th range cell and (c) 12th range cell, (d) Doppler range detection contour for the entire cell ranges.

configuration and ground truth for Scenario A. It is shown from the figure the direct path channel's antenna (marked as Ch1 Antenna) is directed towards the LTE eNB transmitter, while the reflected path channel's antenna (marked as Ch2 Antenna) is directed towards the target area to receive the target echo signals. The real experiment setup for Scenario A is shown in Figure 12, where the positions of Ch1 and Ch2 antennas are illustrated. It is shown from the figure; a shield board is used for Ch2 antenna in order to eliminate the reception of direct signals from LTE eNB. In the Figure 12 the yellow arrows show the antenna's direction.

The detection processing results for the 1st, 6th and 12th range cells are displayed in the Doppler range contours in Figures 13(a), (b) and (c) respectively. The speed of the car and its corresponding Doppler frequency can be calculated from equation:

$$v = fd \cdot c/2fc\cos(\alpha)\cos(\beta/2) \tag{20}$$

where c is the speed of light and f_c the LTE signal carrier frequency. $\alpha\alpha$ and $\beta\beta$ are the relative velocity angle and bistatic angle respectively. In this scenario specifically, at point x of the ground truth (see Figure 11), α and β are estimated at $\alpha \approx 180^\circ$ and $\beta \approx 60^\circ$. Therefore, the detected Doppler frequency at the beginning is -55 Hz (Figure 13(a)) which corresponds to 13 km/h (3.6 m/s), and the negative sign indicates that the car is moving away from the receiver. After a period of acceleration, a -130 Hz Doppler frequency is detected in the 6th range cell (Figure 13(b)) which corresponds to a velocity of about 30 km/h (8.5 m/s). At the 12th range cell, the speed decreased to 28 km/h corresponding to -120 Hz, (Figure 13(c)). It is clear that the car has travelled for ~ 130 m with a non-uniform speed, and this is illustrated in Figure 13(d) which shows the entire cell ranges. These results actually correspond to the controlled speed of the car. From the different speeds, and it is noted that cars with higher speeds can be detected from higher ranges.

5.2. Scenario B

In Scenario B, a car starts moving in straight line from the bistatic receiver's Ch2 antenna and it make a U-turn at around 90 m away from the receiver. The geometric configuration for Scenario B and the Doppler range detection results of the entire cells is illustrated in Figure 14. It can be seen that the car travelled with an average velocity of 10 km/h, and made a U-turn at a range of 90 m. It is noted that the Doppler frequency at 90 m is 0 which was expected at that point (see point y) of Figure 14.

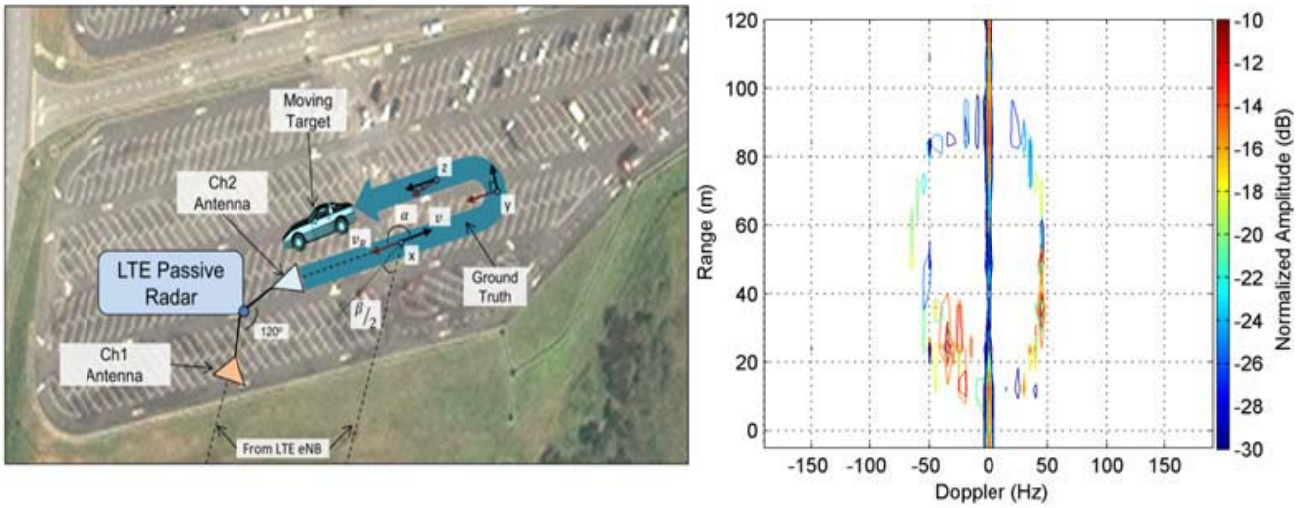

Figure 14. Geometrical configurations for Scenario B and detection processing results display in a Doppler-range contour for the entire ranges cell.

5.3. Scenario C

In Scenario C, a motor bike is used instead of a car as in Figure 15. The motorbike moved in a straight line starting from the receiver's Ch2 antenna until it reached a point of a distance of 130 m, with a speed of around 30 km/h. From the Doppler range detection results of the entire cell ranges it showes that the motor bike has travelled for $\sim$ 130 m with a non-uniform speed ranging from 22–32 km/h (-95–-135 Hz). As the motor bike is smaller in size than a car, it has a smaller RCS but the LTE-based passive radar shows the capability to detect it with a range of $\sim$ 130 m.

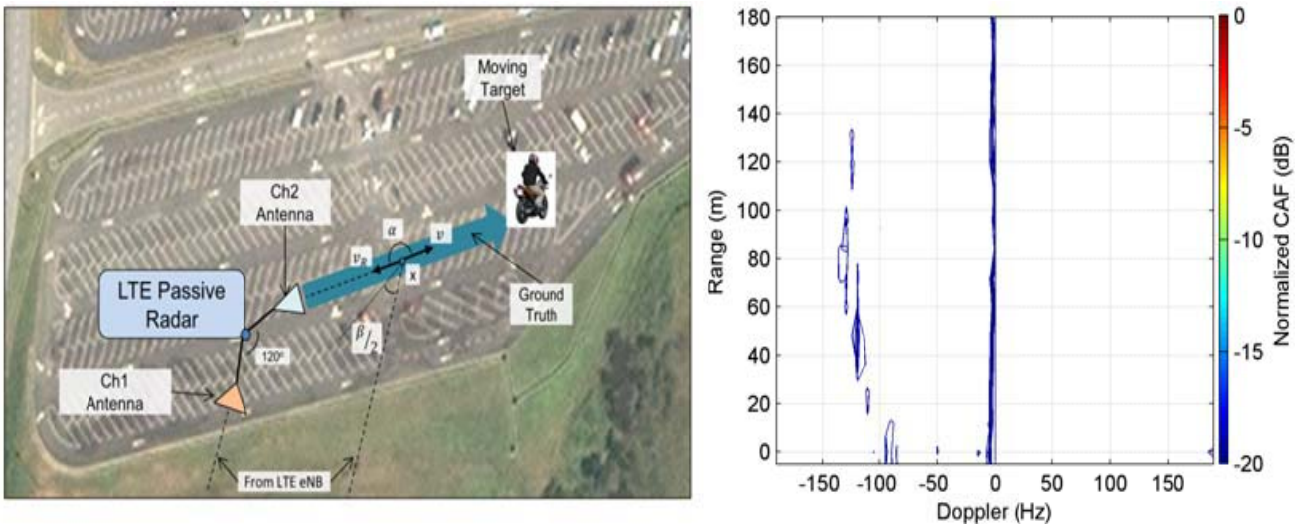

Figure 15. Geometrical configurations for Scenario C and detection results.

5.4. Scenario D

In Scenario D, a human body is used for detection, where a man ran in a straight line starting from the Ch2 antenna up to $\sim$ 60 m, with a speed of $\sim$ 12 km/h. Figure 16 illustrates the geometrical configuration for Scenario D and its Doppler range detection results of the entire cell ranges. It can be predicted that the man was running for $\sim$ 60 m with non-uniform speeds, where he started the run with

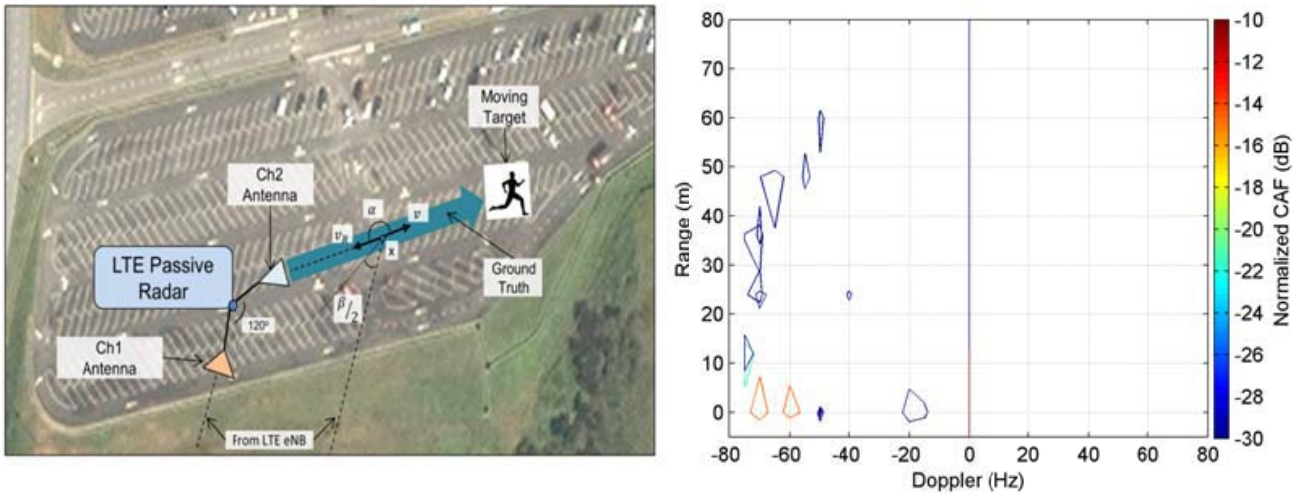

Figure 16. Geometrical configurations Scenario D and detection results.

a velocity of 8 km/h then increased his speed until it reached 15 km/h, and after that his speed started to slow down to prepare for the stop.

5.5. Scenario E

Scenario E is prepared to examine the system's capability to detect two moving targets in the same scene. Two persons (Person1 and Person2) started running from the Ch2 antenna until they reached a point 60 m away. The geometrical configuration for the experiment site of Scenario E and the detection processing results for the 4th, 9th and 13th range cells are illustrated in Figures 17(a), (b) and (c) respectively. In order to examine the LTE signal range resolution (17.3 m) which was calculated in Chapter 3, the two persons are separated with a distance of 20 m, and they ran with different speeds to

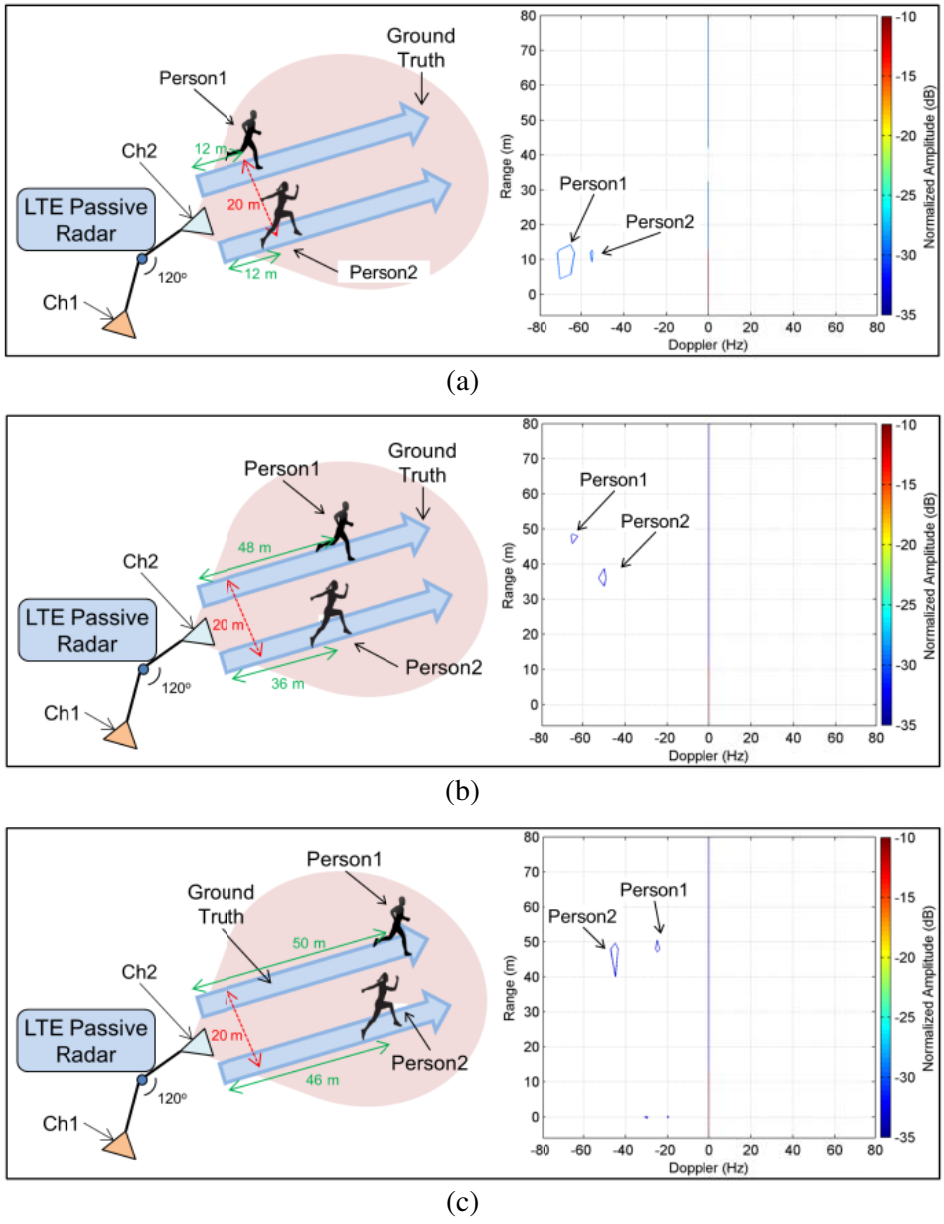

Figure 17. Scenario E: Geometrical configuration and detection results display in a Doppler-range contour for the (a) 4th range cell, (b) 9th range cell, (c) 13th range cell.

examine the calculated Doppler (velocity) resolution (1.18 km/h or 5 Hz). It is shown from Figure 17(a) that both persons are almost at the same range of the receiver (12 m), but the speed of Person1 is higher than Person2, which is $\sim$ 15 km/h (-65 Hz) for Person1 and $\sim$ 13 km/h (-55 Hz) for Person2. The estimated positions for them are illustrated in Figure 17(a). Person1 exceed Person2 in Figure 17(b) where Person1 was detected at a range of 48 m with a speed of 15 km/h while Person2 was detected at a range of 36 m with a speed of 12 km/h. In Figure 17(c), Person1 almost reached his destination at $\sim$ 50 m, and consequently his speed slowed down to 5 km/h (-20 Hz) to prepare for his stop, while Person2 still maintained his speed at 12 km/h.

From the results, it can be deduced that the LTE-based passive radar system can differentiate two moving humans separated by a distance 20 m which is a bit higher than the range resolution (17.3). The two persons had also moved with different speeds, where the two persons' speed difference is 2 km/h which is slightly higher than the LTE velocity resolution (1.3 km/h). Therefore, the system is suitable to be used for monitoring intruders.

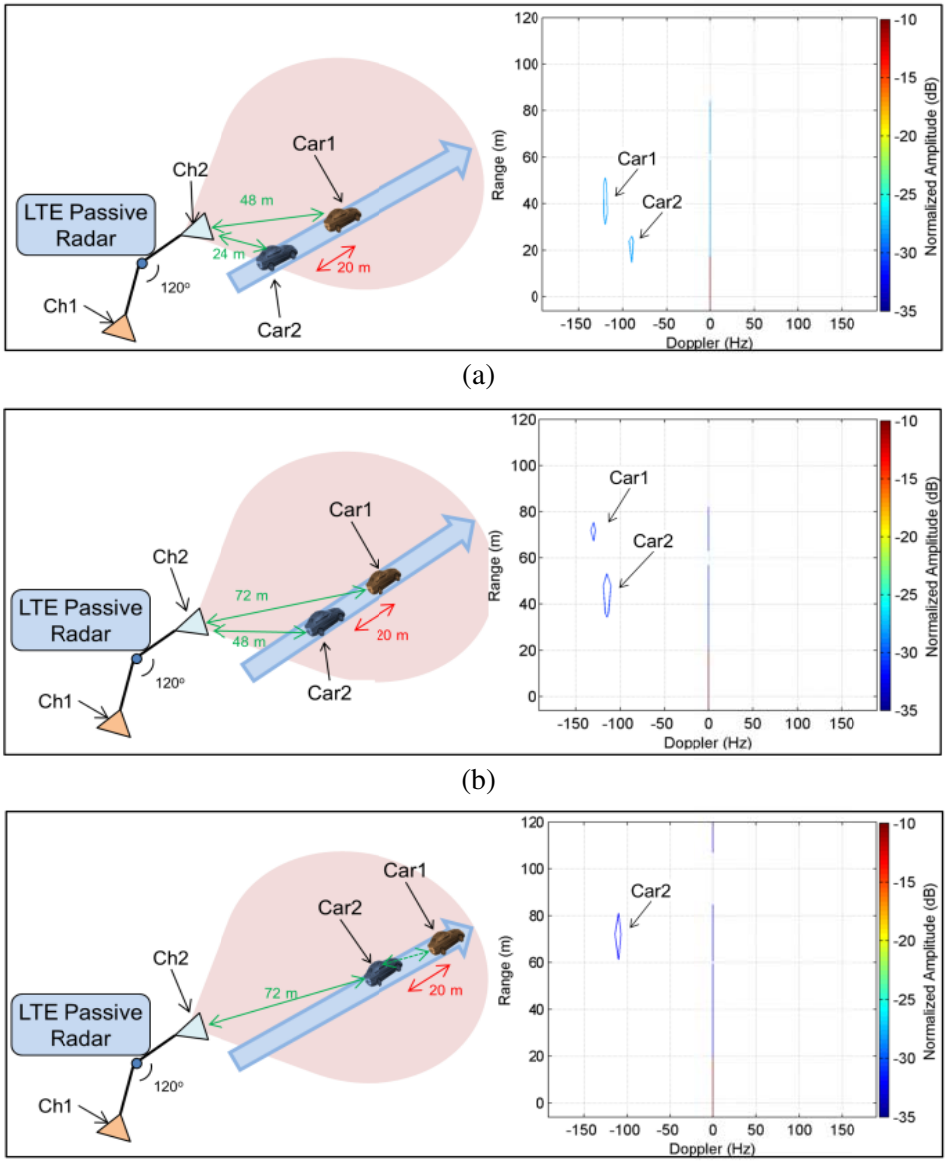

Figure 18. Scenario F: Geometrical configuration and detection results display in a Doppler-range contour for the (a) 7th range cell, (b) 10th range cell, (c) 15th range cell.

5.6. Scenario F

In Scenario F, two cars drove in straight line from Ch2 until they reach ∼ 100 m away. The two cars moved sequentially (Car2 followed Car1), as shown in Figures 18(a), (b) and (c), which illustrate the geometrical configurations for the experiment site and the detection processing results for the 7th, 10th and 15th range cells, respectively. The two cars are separated by 20 m to be beyond the range resolution (17.3 m). It is shown from Figure 18(a) that Car1 exceeded Car2 in range and velocity, where Car1 was detected at 48 m with a velocity of 28 km/h (−120 Hz), while Car2 was detected at ∼ 24 m with a speed of 21 km/h (−90 Hz). The estimated positions for the two cars are illustrated at point A of Figure 18(a). Both cars are detected again in Figure 18(b) but with a higher range and velocity, where Car1 was detected at range ∼ 72 m with a velocity of 32 km/h (−135 Hz), while Car2 is detected at 50 m with a velocity of 28 km/h (−120 Hz). In Figure 18(c) only one car is shown, which corresponds

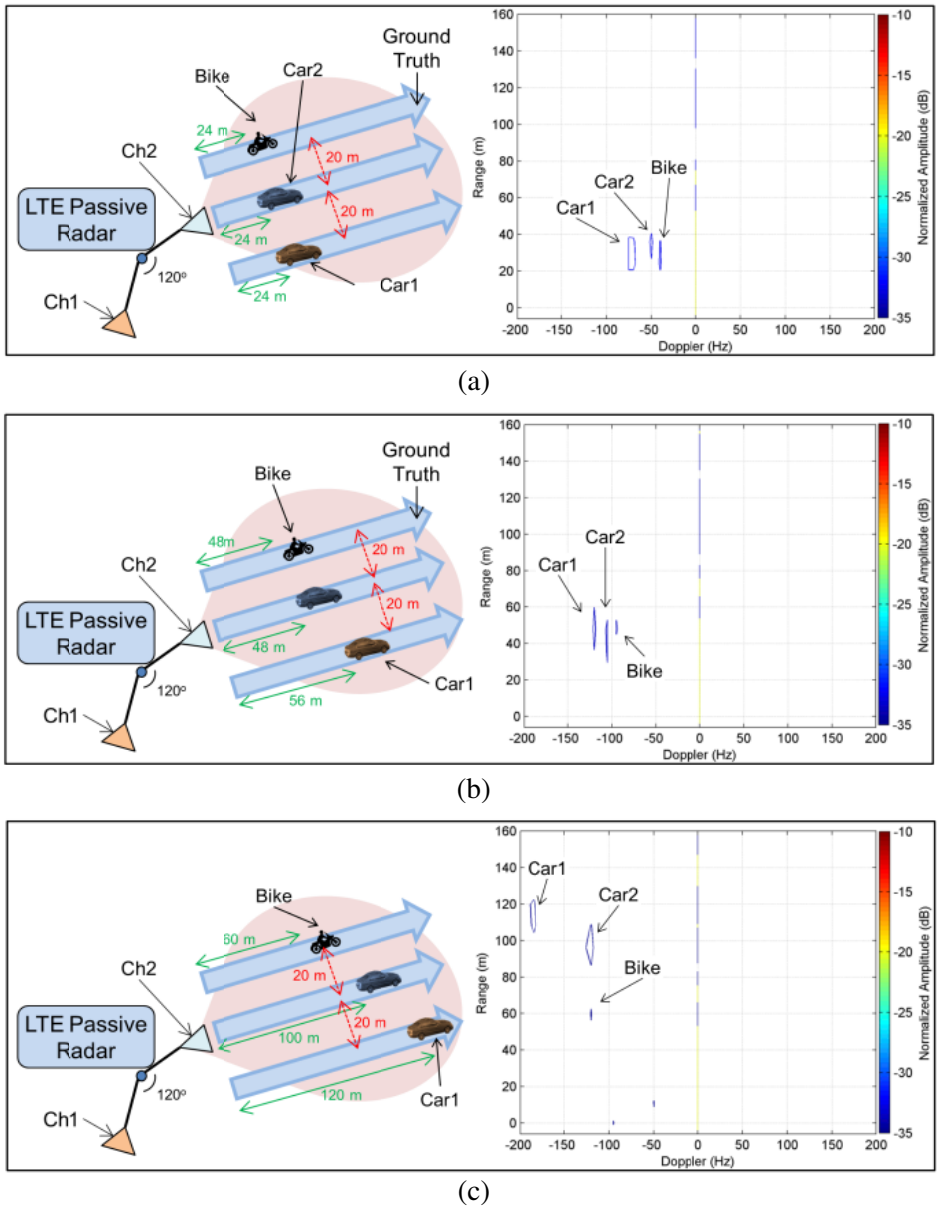

Figure 19. Scenario G: Geometrical configuration and detection results display in a Doppler-range contour for the (a) 5th range cell, (b) 8th range cell, (c) 14th range cell.

to Car2. Car1 is not detected because it is completely hidden by Car2, thus the receiver antenna could not receive the reflected signals by Car1 at this position.

The result of this scenario shows that the LTE-based passive radar can detect and differentiate two cars following each other. The two cars are separated by a distance of 20 m and they moved with varying speeds. That allows the LTE-based passive radar to be used for border protection applications, such as monitoring intruder vehicles.

5.7. Scenario G

In Scenario G, two cars and one motor bike were used in the same scene. The three vehicles traveled from Ch2 antenna to 160 m in a straight line, and they started moving when they are beside each other (parallel). The geometrical configurations for the experiment of Scenario H and the detection processing results for the 5th, 8th and 14th range cells are illustrated in Figure 19. In order to examine the range and Doppler resolutions, the three vehicles were separated by a distance of ~ 20 m which is more than the range resolution (17.3 m) and they had moved with different speeds. It is shown from Figure 19(a) that the three vehicles are detected at the same range of ~ 24 m, but with different velocities. The estimated positions for the three vehicles are illustrated in Figure 19(a), where the speed of Car1 is 16 km/h (-70 Hz) while a record of 12 km/h (-50 Hz) and 10 km/h (-40 Hz) for both Car2 and motor bike were recorded, respectively. In Figure 19(b), as Car1's speed is the highest, it is detected at ~ 56 m with a velocity of 28 km/h (-120 Hz), while both Car2 and motor bike are detected at a range of ~ 48 m with velocities of 25 km/h (-105 Hz) for Car2 and 22 km/h (-95 Hz) for motor bike. It is noted that the motor bike detection peak is smaller because the motor bike has less RCS compared to the cars. In Figure 19(c), the motor bike can still be seen at a range of 60 m with a velocity of 28 km/h (-120 Hz), while Car1 and Car2 are detected at a range of ~ 120 m and ~ 100 m with speeds of 44 km/h (-185 Hz) and 28 km/h (-120 Hz), respectively.

From the results of this scenario it can be deduced that the LTE-based passive radar can detect and differentiate three vehicles separated with a distance a bit higher than the range resolution moving with different speeds, which allows the LTE-based passive radar to be used in traffic speeds surveillance applications.

6. CONCLUSION

LTE-based passive radar is developed, and its capabilities of detecting a ground moving target were tested. The proposed system contains two parallel channels; one dedicated to receive the direct LTE signal from the LTE eNB transmitter and it is called Ch1, while the other is dedicated to receive the signal reflected from the moving target and it is called Ch2. Both channels have the same structure, as they receive the signals through directional antennas which then down-converts the received signals to the baseband before saving them as digital data sets in the PC hard drive. The proposed LTE-based passive radar system performance was evaluated by conducting an outdoor field experiment using a real LTE eNB transmitter as an illumination source. During the experiment, seven scenarios were carried out to investigate the system capability of detecting diverse ground moving targets, move in different speeds and different directions, in addition to examining the system's capability to detect multi-targets moving on the ground in the same scene. The experimental results showed that the LTE-based passive radar system has the capability of detecting a car, motor bike or even a human body moving with varying speeds including 10, 20, 30 and 40 km/h, and they are detected with different ranges, from 0–160 m. Therefore, from the results presented in this paper, there is no doubt that the LTE-based passive radar has a high capability of detecting different types of ground moving targets including cars, motor bikes and humans, which makes the LTE-based passive radar system suitable for many applications including and not limited to: traffic speed surveillance, border protection and monitor of buildings. In spite of the positive results obtained, it should be pointed out that there is still a need for further studies and improvements. A future study could include the system's capability for tracking different types of objects. Also, more advanced signal processing algorithms could be applied to improve tracking accuracy, as an example reference [18] applied Multiple Input Multiple Output (MIMO) technique for ship detection and tracking in high frequency (HF) Radar systems.

REFERENCES

1. Griffiths, H. and N. Long, "Television-based bistatic radar," *IEE Proceedings (Communications, Radar and Signal Processing)*, 1986.
2. Howland, P. E., D. Maksimiuk, and G. Reitsma, "FM radio based bistatic radar," *IEEE Aerospace and Electronic Systems Magazine*, 107–111, 2005.
3. Poullin, D., "Passive detection using digital broadcasters (DAB, DVB) with COFDM modulation," *IEE Proceedings in Radar, Sonar and Navigation*, 2005.
4. Griffiths, H., et al., "Bistatic radar using satellite-borne illuminators of opportunity," *IET International Conference in Radar*, Vol. 92, 1992.
5. Guo, H., K. Woodbridge, and C. Baker, "Evaluation of WiFi beacon transmissions for wireless based passive radar," *IEEE Radar Conference (RADAR)*, 2008.
6. Falcone, P., et al., "Localization and tracking of moving targets with WiFi-based passive radar," *IEEE Radar Conference (RADAR)*, 2012.
7. Tan, D. K. P., H. Sun, Y. Lu, M. Lesturgie, and H. L. Chan, "Passive radar using global system for mobile communication signal: Theory, implementation and measurements," *IEE Proceedings in Radar, Sonar and Navigation*, 2005.
8. Sun, H., D. K. P. Tan, and Y. Lu, "Aircraft target measurements using a GSM-based passive radar," *IEEE Radar Conference (RADAR)*, 2008.
9. Wang, Q., C. Hou, and Y. Lu, "An experimental study of WiMAX-based passive radar," *IEEE Transactions on Microwave Theory and Techniques*, Vol. 58, No. 12, 3502–3510, 2010.
10. Sinha, N. B., et al., "Target localization accuracy using WiMAX radar networks," *Journal of Theoretical & Applied Information Technology*, Vol. 27, No. 2, 2011.
11. Chadchan, S. and C. Akki, "3GPP LTE/SAE: An overview," *International Journal of Computer and Electrical Engineering*, Vol. 2, No. 5, 806–814, 2010.
12. Salah, A. A., R. S. A. Raja Abdullah, A. Ismail, F. Hashim, C. Y. Leow, M. B. Roslee, and N. E. A. Rashid, "Feasibility study of LTE signal as a new illuminators of opportunity for passive radar applications," *2013 IEEE International RF and Microwave Conference (RFM)*, 2013.
13. Salah, A. A., R. S. A. Raja Abdullah, A. Ismail, and F. Hashim, "Experimental study of LTE signals as illuminators of opportunity for passive bistatic radar applications," *Electronics Letters*, Vol. 50, No. 7, 545–547, 2014.
14. Mohammadpoor, M., R. S. A. Raja Abdullah, A. Ismail, and A. F. Abas, "A circular synthetic aperture radar for on-the-ground object detection," *Progress In Electromagnetics Research*, Vol. 122, 269–292, 2012.
15. Cherniakov, M., R. S. A. Raja Abdullah, P. Jancovic, M. Salous, and V. Chapursky, "Automatic ground target classification using forward scattering radar," *IEE Proceedings in Radar, Sonar and Navigation*, Vol. 153, 427–437, 2006.
16. Kvaksrud, T.-I., "Range measurements in an open field environment," *Texas Instrum*, Incorporated, Dallas, TX, Design Note DN018, 2008.
17. Shi, Z.-G., S. Qiao, K. S. Chen, W.-Z. Cui, W. Ma, T. Jiang, and L.-X. Ran, "Ambiguity functions of direct chaotic radar employing microwave chaotic colpitts oscillator," *Progress In Electromagnetics Research*, Vol. 77, 1–14, 2007.
18. Dzvonkovskaya, T. Helzel, L. Petersen, C. R. Merz, Y. Liu, and R. H. Weisberg, "Initial results of ship detection and tracking using WERA HF ocean radar with MIMO configuration," *15th International Radar Symposium (IRS)*, 2014.